applied sciences

MDPI

Article

Temperature-Dependent Electrical Properties of Al_2O_3-Passivated Multilayer MoS_2 Thin-Film Transistors

Seok Hwan Jeong, Na Liu, Heekyeong Park, Young Ki Hong * and Sunkook Kim *

School of Advanced Materials Science and Engineering, Sungkyunkwan University, Suwon, Kyunggi-do 16419, Korea; csh0122@skku.edu (S.H.J.); naliufit9@gmail.com (N.L.); parkpa19@skku.edu (H.P.)

* Correspondence: imhyke0419@gmail.com (Y.K.H.); seonkuk@skku.edu (S.K.); Tel.: +82-31-290-7408 (S.K.)

Received: 1 February 2018; Accepted: 8 March 2018; Published: 12 March 2018

Abstract: It is becoming more important for electronic devices to operate stably and reproducibly under harsh environments, such as extremely low and/or high temperatures, for robust and practical applications. Here, we report on the effects of atomic-layer-deposited (ALD) aluminum oxide (Al_2O_3) passivation on multilayer molybdenum disulfide (MoS_2) thin-film transistors (TFTs) and their temperature-dependent electrical properties, especially at a high temperature range from 293 K to 380 K. With the aid of ultraviolet-ozone treatment, an Al_2O_3 layer was uniformly applied to cover the entire surface of MoS_2 TFTs. Our Al_2O_3-passivated MoS_2 TFTs exhibited not only a dramatic reduction of hysteresis but also enhancement of current in output characteristics. In addition, we investigated the temperature-dependent behaviors of the TFT performance, including intrinsic carrier mobility based on the Y-function method.

Keywords: transition metal dichalcogenide; molybdenum disulfide; thin-film transistor; passivation; contact resistance; intrinsic mobility

1. Introduction

With the discovery of graphene, two-dimensional (2D) layered materials have been drawing intense research interest. Despite its excellent mechanical, optical, and electrical properties, however, graphene is considered unsuitable as an active component of field effect transistors due to its lack of a band gap [1–3]. In efforts to overcome this limitation, i.e., to produce a band gap in graphene, a great deal of research has been carried out, but the results thus far have only added to the complexity of the processes and reduced mobility [4,5].

In this context, layered 2D transition metal dichalcogenides (TMDs)-based thin-film transistors (TFTs) are drawing considerable attention as promising candidates to lead the next-generation transistor technology. Among the 2D TMDs, molybdenum disulfide (MoS_2) is at the center of attention, and relevant research is underway [6–8]. MoS_2 TFTs have excellent carrier mobility, a high on- and off-current ratio (I_{on}/I_{off}), mechanical flexibility, and a relatively large band gap [9–12]. Despite these properties, when the MoS_2 channel is exposed to atmospheric environments, MoS_2 TFTs exhibit a hysteresis phenomenon in the transfer characteristic. Various research groups have already shown that this hysteresis phenomenon occurs in MoS_2 TFTs due to the effects of oxygen and water in the air [13–15]. To suppress this phenomenon, the surface of a semiconducting active channel must be isolated from the air by passivation layers, e.g., atomic-layer-deposited (ALD) aluminum oxide (Al_2O_3) or hafnium dioxide.

It is known that the surface of pristine (i.e., without any surface modifications) MoS_2 does not react well with trimethylaluminum (TMA), which is used as a precursor to form Al_2O_3 layers, due to the absence of dangling bonds [16–19]. However, high-k dielectric layers without pinholes and/or cracks are indispensable for nano-electronic devices. To improve the wettability and reactivity between the MoS_2 surface and TMA and to ensure complete isolation of the surface from atmospheric environments, some strategies prior to deposition of the passivation layer were proposed, for example, oxygen plasma or ultraviolet-ozone (UV-ozone) treatment [18–23]. Conventional MoS_2 TFTs without passivation layers exhibited different electrical properties at high temperatures with respect to the height of the Schottky barrier between the metal electrodes and MoS_2 [8,24,25]. For a relatively high Schottky barrier, charge carriers (i.e., electrons) were blocked by the barrier and thus could not pass at a low temperature. However, as the temperature increased, those carriers started to transport into the MoS_2 channels through thermionic emission [26]. This led to an increase in carrier mobility with respect to increased temperature. Unlike previous reports on MoS_2 TFTs, little research has been conducted on the transport mechanism at high temperatures in passivated MoS_2 TFTs.

The present study investigated how passivated MoS_2 TFTs with a high Schottky barrier change in a high-temperature environment. First, cross-sectional transmission electron microscopy (TEM) was utilized to visualize the quality of Al_2O_3 deposited on the MoS_2 surface through UV-ozone treatment. The surface morphology of the Al_2O_3 on the MoS_2 channel was investigated by atomic force microscopy (AFM), depending on UV-ozone treatment. Also, the electrical properties of the devices were characterized to assess the effectiveness of Al_2O_3 passivation. As a result, it was confirmed that carrier mobility improved and that the hysteresis effect decreased significantly; thus, the desired effect of passivation was achieved. After that, the same tests were performed while the temperature was increased from room temperature to 380 K, and the results showed that the mobility also increased with increasing TFT operating temperature. To analyze the increment of the mobility, the *Y*-function method was employed to examine the intrinsic mobility of the MoS_2 TFT by excluding contact resistance between the metal electrode and MoS_2 channel.

2. Materials and Methods

2.1. Device Fabrication

Multilayer MoS_2 flakes were mechanically exfoliated from bulk MoS_2 (SPI Supplies, West Chester, PA, USA) through the conventional Scotch tape method and transferred onto thermally grown silicon dioxide (SiO_2) with a thickness of 300 nm used as a gate insulator. A *p*-type doped silicon (Si) wafer (resistivity $\leq$0.005 Ω·cm) was used as a gate electrode and substrate. To remove the organic and inorganic residues resulting from the transfer procedure, the MoS_2-covered SiO_2/Si substrate was cleaned in acetone and isopropyl alcohol for 1 h 30 min and 30 min, respectively. Titanium/gold (20 nm/100 nm) layers were sequentially deposited by electron beam (e-beam) evaporation, and then source/drain (S/D) electrodes were patterned through conventional photolithography and wet etching processes. To improve the contact between the S/D electrodes and MoS_2 active channel, the devices were annealed at 200 °C for 2 h under mixed gas flow (100 sccm of Ar/10 sccm of H_2).

2.2. UV-Ozone Treatment

For uniform growth of the Al_2O_3 layer, as-fabricated MoS_2 TFTs were subjected to UV-ozone treatment (UVC-30, Jaesung Engineering Co., Anyang-Si, Korea) at power of 15 to 25 mW for 5 min with wavelengths of 185 nm and 254 nm.

2.3. ALD Al_2O_3 Passivation

An Al_2O_3 layer was deposited on the UV-ozone-treated MoS_2 TFTs by ALD (Lucida D100, NCD Co., Ltd., Daejeon, Korea). The deposition conditions of the unit ALD sequence consisted of TMA (0.2 s)/N_2 (10 s)/H_2O (0.2 s)/N_2 (10 s) with a chamber temperature of 200 °C. The thickness of the deposited Al_2O_3 per unit sequence was controlled to be approximately 0.118 nm. The unit sequence was iterated 340 times for a target thickness of 40 nm.

Then a selected area in the Al_2O_3 deposited on the S/D electrode was eliminated to create the electrical contact during measurements.

2.4. Device Characterization

The cross section of the Al_2O_3-passivated MoS_2 TFT was analyzed by TEM (Titan Cubed 60-300, FEI, Hillsboro, OR, USA). The surface morphologies of the Al_2O_3 on MoS_2 TFTs were investigated by AFM (XE7, Park Systems, Suwon-si, Korea) with noncontact mode operation. The electrical properties of the MoS_2 TFTs were measured by using a semiconductor characterization system (4200 SCS, Keithley, Cleveland, Ohio, USA) with a probe station. The temperature dependence of the TFT performance was characterized by using a home-made temperature-controlling vacuum chamber with temperatures ranging from 293 K to 380 K under a moderate vacuum environment (<10^{-3} torr). Before each measurement, the temperature was maintained for 10 min to minimize variations in device performance.

3. Results and Discussion

Figure 1a shows a three-dimensional (3D) schematic illustration of the back-gated TFT encapsulated with Al_2O_3 on top of the multilayer MoS_2 active channel, which was also confirmed in a top-view optical microscope image, as shown in Figure 1b. MoS_2 and contact holes in the S/D electrodes are indicated by red dashed and green dotted lines, respectively. It should be noted that we could not find any pinholes or cracks in the Al_2O_3 layer resulting from UV-ozone pre-treatment, which will be further discussed in relation to Figure 2. Channel length (L) and width (W) of the MoS_2 device were 13.06 and 20.32 μm, respectively, used for calculating the TFT performance in relation to various temperatures.

Figure 1c shows a cross-sectional TEM image of the Al_2O_3-encapsulated MoS_2 TFT with UV-ozone pretreatment. It can be seen that the Al_2O_3 with an average thickness of approximately 42.0 nm uniformly covered the entire MoS_2 surface. In addition, the thickness of the MoS_2 multilayer was estimated to be approximately 64.6 nm, indicating its nearly bulk-like energy band characteristics. The fast Fourier transform patterns and high-angle annular dark-field imaging of the MoS_2 are shown in Figure S1 in the Supplementary Materials.

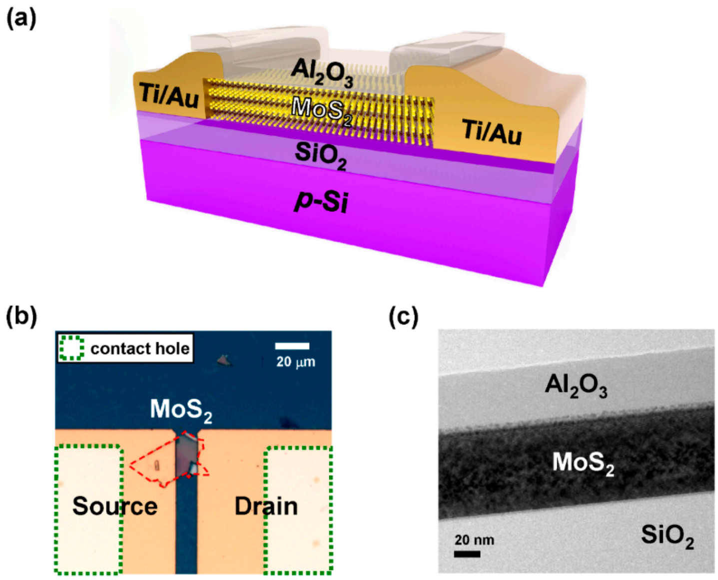

Figure 1. (**a**) 3D schematic structure of multilayer molybdenum disulfide (MoS_2) thin-film transistor (TFT) passivated with aluminum oxide (Al_2O_3); (**b**) optical microscope and (**c**) cross-sectional transmission electron microscopy (TEM) images of the MoS_2 TFT with Al_2O_3 passivation, respectively.

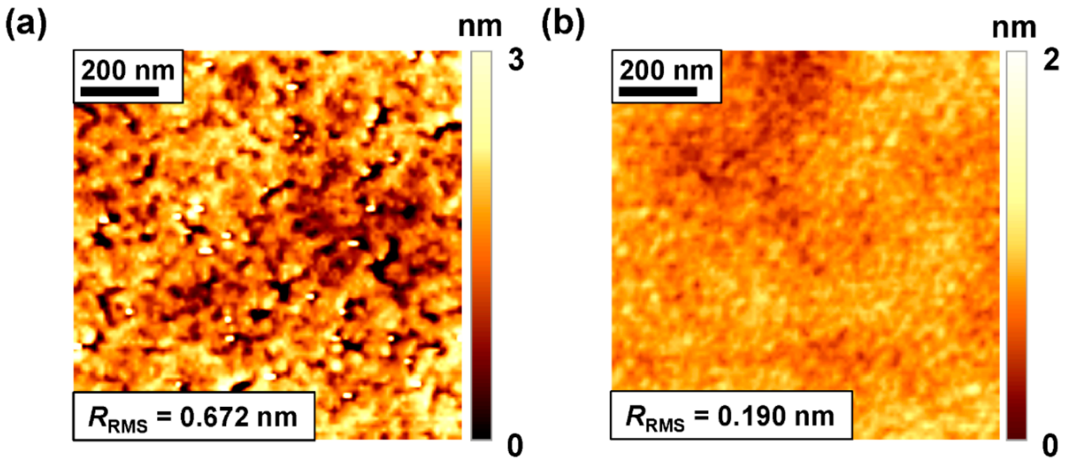

Figure 2. Atomic force microscopy (AFM) images of Al_2O_3 surfaces on MoS_2 active channel: (**a**) without and (**b**) with ultraviolet-ozone (UV-ozone) treatment for 5 min before atomic-layer-deposited (ALD) procedure. RMS: root-mean-square.

Figure 2 compares the surfaces morphologies of the Al_2O_3 deposited on MoS_2 with and without UV-ozone pretreatment, which were measured by AFM scanning in a 1 µm × 1 µm region. Many clusters and boundaries can be observed on the surface of the Al_2O_3 (thickness of approximately 40 nm) deposited on the pristine MoS_2 (Figure 2a). However, in the case of Al_2O_3 deposited on the MoS_2 with UV-ozone pretreatment, it shows complete coverage with high uniformity (Figure 2b). The root-mean-square surface roughness (R_{RMS}) of the directly deposited Al_2O_3 is 0.672 nm, but it decreases to 0.190 nm with a 5-min UV-ozone treatment on MoS_2. These results indicate that UV-ozone exposure is an efficient way to achieve uniform growth of Al_2O_3 on a MoS_2 surface.

Previous studies have found that the electrical properties and device performance of MoS_2 transistors can be enhanced by high-k dielectric encapsulation [27,28]. Therefore, we measured the electrical properties of the MoS_2 TFTs to elucidate the effect of Al_2O_3 passivation on multilayer MoS_2 with UV-ozone pretreatment. Figure 3a compares the transfer characteristic curves $I_{ds}-V_{gs}$ of the MoS_2 TFTs without and with Al_2O_3 passivation layers with the application of a source-to-drain voltage (V_{ds}) of 1 V. Before Al_2O_3 passivation, the pristine MoS_2 TFT exhibits a large hysteresis (black-solid lines in Figure 3a). However, after Al_2O_3 passivation with UV-ozone pre-treatment, represented by the red solid lines in Figure 3a, the transfer curve obtained from a forward V_{gs} scan closely approached that obtained from a reverse V_{gs} scan and vice versa, which indicates a distinct reduction of hysteresis behavior (see also Figure S3). It should be noted that reduction of hysteresis was not observed in the MoS_2 TFTs with only UV-ozone treatment, i.e., without Al_2O_3 passivation (Figure S4). For quantitative comparison, we define the difference of threshold voltage (ΔV_{th}) by subtraction between the V_{th} values in the forward and reverse transfer characteristic curves, which are estimated to be 20.1 V and 0.5 V for the pristine and Al_2O_3-passivated devices, respectively. However, I_{off} in the Al_2O_3-passivated MoS_2 TFT increased by about one order of magnitude, resulting in a decrease in the I_{on}/I_{off} from 10^6 to 10^5. The results may be attributed to the fact that excess electrons could be induced in the MoS_2 active channel due to the positive fixed charges in the Al_2O_3 layer [23,28].

According to transport physics in TFTs, the relation among I_{ds}, V_{gs} and V_{ds} are expressed for a linear regime ($|V_{ds}| < |V_{gs} - V_{th}|$) as in [29]:

$$I_{ds} = \frac{\mu_{eff} W C_{GI}}{L} \left[(V_{gs} - V_{th}) V_{ds} - \frac{V_{ds}^2}{2} \right], \quad (1)$$

where C_{GI} is capacitance per unit area of the gate insulator, and μ_{eff} is the field-effect mobility, one of the figure-of-merit for evaluating TFT characteristics. Based on the standard model of metal-oxide-semiconductor (MOS) FETs and a parallel plate model of gate capacitance [8,29,30], μ_{eff} of the TFT can be expressed in terms of transconductance ($g_m \equiv \partial I_{ds}/\partial V_{gs}$) as

$$\mu_{eff} = \frac{L g_m}{W C_{ox} V_{ds}}, \tag{2}$$

where C_{ox} is capacitance per unit area of gate insulator (1.15×10^{-8} Fcm^{-2}). The maximum transconductance of the pristine MoS_2 TFT was 2.31×10^{-7} S, which was increased to 3.25×10^{-7} S after Al_2O_3 passivation. As a result, the μ_{eff} values for the pristine and Al_2O_3-passivated MoS_2 TFTs were calculated to be 40.9 cm^2 V^{-1} s^{-1} and 57.6 cm^2 V^{-1} s^{-1}, respectively. Figure 3b compares the output characteristic curves ($I_{ds}-V_{ds}$) of the MoS_2 TFTs without and with Al_2O_3 passivation layers under the application of V_{gs} ranging from −30 V to 0 V with a step of 5 V. At a low V_{gs} range from −30 V to −15 V, the I_{ds} values of the Al_2O_3-passivated MoS_2 TFTs were slightly lower than those of the pristine MoS_2 TFT. However, the clear enhancement of the I_{ds} of the passivated device has been observed at higher V_{gs} than −10 V, which agrees well with Figure 3a.

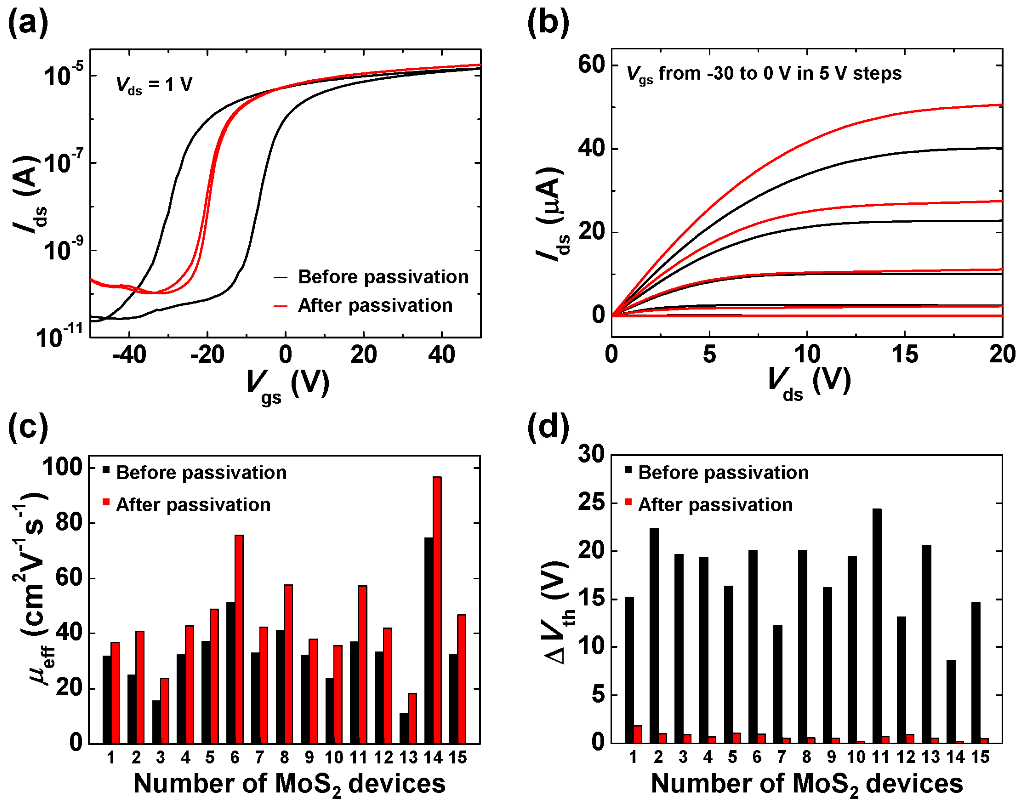

Figure 3. Comparisons of (**a**) transfer and (**b**) output characteristics of MoS_2 TFTs with respect to Al_2O_3 passivation. Variations of (**c**) field-effect mobility (μ_{eff}) and (**d**) threshold voltage (ΔV_{th}) of 15 representative Al_2O_3-passivated MoS_2 TFTs compared with those of pristine devices. All the Al_2O_3 layers were deposited after UV-ozone treatment.

It is well known that MoS_2 seems to be very sensitive to oxygen and water when exposed to an ambient environment [31]. Oxygen and water molecules can be adsorbed on the defect sites of MoS_2 to induce charge traps, thus leading to a relatively larger and clockwise hysteresis as well as mobility degradation [13,32]. High-k dielectric passivation through ALD can be suggested as an efficient method to isolate MoS_2 from atmospheric environments that include external contaminants [27,28,33]. The enhanced I_{ds} is also attributed to the annealing effect, which decreases the contact resistance between the S/D electrodes and MoS_2 surface. These results are consistent with those of previous reports on Al_2O_3-encapsulated MoS_2 devices, which indicates that no significant defect was introduced in the MoS_2 by the UV-ozone treatment [27,28]. The MoS_2 surface before and after UV-ozone treatment were investigated using Raman and X-ray photoelectron spectroscopy (shown in Figure S2).

Figure 3c,d show the statistical distributions of μ_{eff} and ΔV_{th} for 15 representative MoS_2 TFTs in order to confirm the effect of UV-ozone pre-treatment followed by Al_2O_3 passivation. The results of all the devices exhibit increments of the μ_{eff} as well as reduction of the ΔV_{th}. The average increment (reduction) rate of μ_{eff} (ΔV_{th}) is 40.4% (4.2%). The individual values of μ_{eff} and ΔV_{th} are listed in Table 1. These results are evidence that UV-ozone treatment of the multilayer MoS_2 TFTs not only improves the quality of the ALD-grown Al_2O_3 layer, but also enhances the mobility and stability of the MoS_2 devices.

Table 1. Comparison of μ_{eff} and ΔV_{th} values of 15 representative Al_2O_3-passivated MoS_2 TFTs. [1]

# of TFT	μ_{eff} (cm^2 V^{-1} s^{-1})		ΔV_{th} (V)	
	Before	After	Before	After
1	31.58	36.57	15.16	1.79
2	24.79	40.55	22.33	0.98
3	15.49	23.58	19.66	0.87
4	32.07	42.59	19.32	0.64
5	36.99	48.52	16.32	1.04
6	51.19	75.53	20.05	0.94
7	32.79	42.18	12.25	0.5
8	40.93	57.62	20.09	0.54
9	31.87	37.79	16.18	0.51
10	23.49	35.55	19.43	0.17
11	36.83	57.22	24.37	0.72
12	33.14	41.69	13.08	0.87
13	10.82	18.19	20.61	0.53
14	74.57	96.67	8.58	0.15
15	32.11	46.63	14.6	0.47

[1] All the Al_2O_3 layers were deposited after UV-ozone treatment.

To demonstrate the temperature-dependent behavior of the Al_2O_3-passivated MoS_2 TFT, the electrical properties of the device were measured at 10 different temperatures ranging from 293 K to 380 K under a moderate vacuum condition. Figure 4a presents a semi-logarithmic-scale plot of the temperature-dependent transfer characteristic curves at five different temperatures (293, 310, 330, 350 and 370 K). At the semi-logarithmic-scale of I_{ds}, variation of I_{on} was not clearly distinguished. To reveal the enhancement of I_{on}, linear scale plots of the transfer curves at five other temperatures (300, 320, 340, 360 and 380 K) are compared in Figure 4b.

As shown in Figure 4, I_{ds} increased with increasing temperature over the whole V_{gs} region. The results also confirmed the linear increment of the I_{ds} values at a V_{gs} of 40 V with respect to 10 different temperatures, as shown in the inset of Figure 4a. From the transfer characteristic curves, we extracted the V_{th} at 10 different temperatures, which linearly shifted toward the negative V_{gs} region with increasing temperature (inset of Figure 4b).

Figure 5a shows the output characteristics of the Al_2O_3-passivated MoS_2 TFT at 293 K with those at 380 K, which exhibits almost double increments of I_{ds}. The results also imply that high temperature would influence the other aspects of TFT performance. However, our TFT architecture has a two-terminal configuration resulting in contact resistance between the S/D electrodes and the MoS_2 active channel, which should be minimized for further investigation of carrier transport mechanisms.

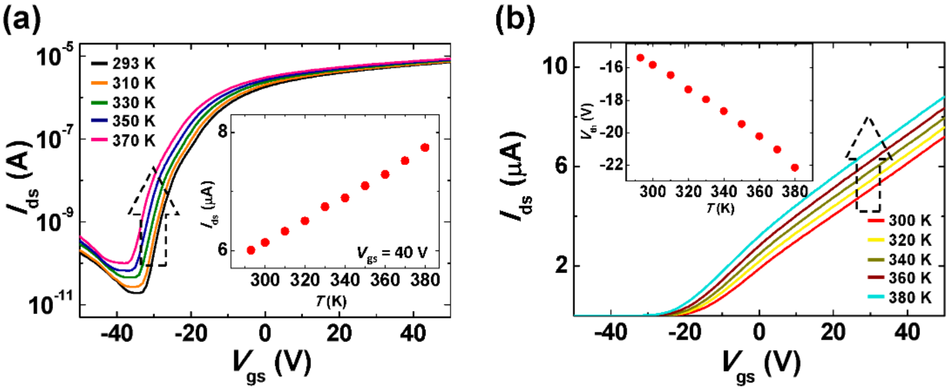

Figure 4. Transfer characteristics of Al_2O_3-passivated MoS_2 TFT under various temperatures ranging from 293 K to 380 K in (**a**) logarithmic and (**b**) linear scales. Insets: temperature-dependent variations of (**a**) I_{ds} at V_{gs} = 40 V and (**b**) V_{th}.

In this context, the Y-function method can be suggested as a proper solution for handling contact resistance in two-terminal systems [8,34–37], which underestimates the intrinsic capabilities of active materials. By adopting the mobility reduction coefficient η [34], Equation (1) can be rewritten as

$$I_{\mathrm{ds}} = \frac{WC_{\mathrm{GI}}}{L} \frac{\mu_0}{\left[1+\eta\left(V_{\mathrm{gs}} - V_{\mathrm{th}}\right)\right]}\left(V_{\mathrm{gs}} - V_{\mathrm{th}}\right)V_{\mathrm{ds}}\,, \tag{3}$$

where μ_0 is the intrinsic mobility excluding any contact resistance component. Considering the definition of transconductance, g_{m} is also modified using η as follows:

$$g_{\mathrm{m}} \equiv \frac{\partial I_{\mathrm{ds}}}{\partial V_{\mathrm{gs}}} = \frac{WC_{\mathrm{GI}}}{L} \frac{\mu_0}{\left[1+\eta\left(V_{\mathrm{gs}} - V_{\mathrm{th}}\right)\right]^2} V_{\mathrm{ds}}\,. \tag{4}$$

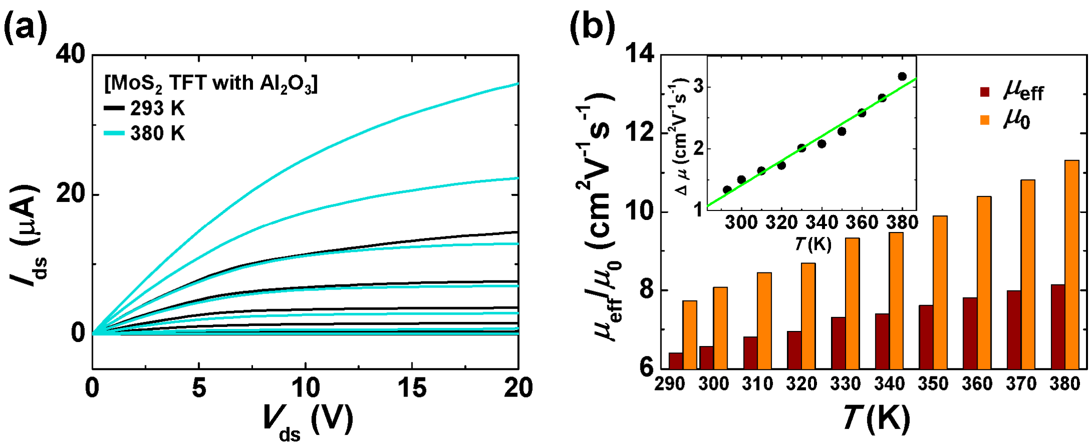

Figure 5. (**a**) Output characteristics of Al_2O_3-passivated MoS_2 TFT under different temperatures of 293 K and 380 K (V_{gs} from −40 to 0 V in 5 V steps); (**b**) comparison of μ_{eff} and the intrinsic carrier mobility μ_0 at various temperatures ranging from 293 K to 380 K. Inset: temperature-dependent variations of the difference between μ_{eff} and μ_0 ($\Delta\mu$).

Then, η is eliminated by combining Equations (3) and (4), and the Y-function can be expressed as

$$Y \equiv \frac{I_{\mathrm{ds}}}{\sqrt{g_{\mathrm{m}}}} = \sqrt{\frac{W}{L}C_{\mathrm{GI}}\mu_0 V_{\mathrm{ds}}} \times \left(V_{\mathrm{gs}} - V_{\mathrm{th}}\right). \tag{5}$$

Finally, we can extract the intrinsic carrier mobility μ_0 from the slope of the $Y-V_{gs}$ plot [8].

Figure 5b presents μ_{eff} and μ_0 of the Al_2O_3-passivated MoS_2 TFT at various temperatures, which were calculated from Equations (2) and (5), respectively. At all temperatures, the results showed that (i) all μ_0 values were higher than μ_{eff}, indicating the existence of relatively high Schottky barriers and subsequent contact resistances in our devices; and (ii) both μ_{eff} and μ_0 gradually increased with increasing temperature, which can be attributed to reduction of the contact resistance and increased thermionic emission due to high temperature [25,38]. The inset of Figure 5b presents the temperature-dependent variation of the difference between μ_{eff} and μ_0 ($\Delta\mu$), which shows linear response behavior with respect to temperature increase. The details of μ_{eff}, μ_0 and $\Delta\mu$ are provided in Table 2.

Table 2. Values of μ_{eff} and μ_0 at various temperatures.

Temperature	293 K	300 K	310 K	320 K	330 K	340 K	350 K	360 K	370 K	380 K
μ_{eff}	6.4	6.57	6.81	6.95	7.31	7.39	7.61	7.81	7.99	8.14
μ_0	7.73	8.07	8.45	8.68	9.32	9.47	9.89	10.39	10.81	11.31
$\Delta\mu$	1.33	1.5	1.64	1.73	2.01	2.08	2.28	2.58	2.82	3.17

4. Conclusions

In this paper, we reported on the effects of ALD-Al_2O_3 passivation on multilayer MoS_2 TFTs and the temperature-dependent variation of the TFT performance. High-k Al_2O_3 layers were uniformly passivated over the entire surface of MoS_2 TFTs with the aid of UV-ozone treatment leading to (i) huge reductions of the hysteretic transfer curves; (ii) saturation current enhancement of the output characteristics; and (iii) increases in μ_{eff} of approximately 40.4%. Based on investigations of the temperature-dependent TFT characteristics including intrinsic carrier mobility (μ_0) extracted by the Y-function method, we could conclude that the dominant transport mechanism is thermionic emission in our Al_2O_3-passivated MoS_2 TFTs with a considerable Schottky barrier between the S/D electrodes and active channel. In addition, the proposed approach at relatively high (i.e., realistic device working) temperatures can be employed to realize stable and reproducible electronic devices for robust and practical applications.

Supplementary Materials: The following are available online at www.mdpi.com/2076-3417/8/3/424/s1, Figure S1: (**a**) Cross-sectional TEM image of a MoS_2 encapsulated by Al_2O_3. Inset: FFT patterns of the MoS_2 obtained in the area marked with the white dashed line. (**b**) HAADF image of a MoS_2 TFT with Al_2O_3 passivation; (**c**) atomic percentage of the atoms contained in the area marked with red and green rectangles in (**b**). Figure S2: Raman and (**b**) XPS spectra of (i) pristine and (ii) UV-ozone treated MoS_2. Figure S3: Transfer characteristics of 14 MoS_2 TFTs before (black line) and after (red line) Al_2O_3 passivation., Figure S4: Transfer characteristics of six MoS_2 TFTs without Al_2O_3 passivation before (i.e., pristine) and after UV-ozone treatment.

Acknowledgments: This research was supported in part by a National Research Foundation of Korea (NRF) grant funded by the Korean government (Ministry of Science and ICT, MSIT) (No. 2016R1C1B1016344, 2015R1A1A1A05027488) and the Ministry of Trade, Industry and Energy and Korea Evaluation Industrial Technology through the Industrial Strategic Technology Development Program (No. 10079571, 10080348). Support from the Korea Research Fellowship program funded by the MSIT and Future Planning through the NRF (No. 2017H1D3A1A02014116) and the Basic Science Research Program through the NRF funded by the Ministry of Education (No. 2017R1D1A1B030353150) is also gratefully acknowledged.

Author Contributions: Y.K.H. and S.K. conceived and designed the experiments. S.H.J. and H.P. performed the experiments. Y.K.H., S.K. and N.L. analyzed the results. All the authors wrote and reviewed the manuscript. S.H.J. and N.L. contributed to this work equally.

Conflicts of Interest: The authors declare no conflict of interest.

References

1. Novoselov, K.S.; Geim, A.K.; Morozov, S.V.; Jiang, D.; Katsnelson, M.I.; Grigorieva, I.V.; Dubonos, S.V.; Firsov, A.A. Two-dimensional gas of massless Dirac fermions in graphene. *Nature* **2005**, *438*, 197–200. [CrossRef] [PubMed]

2. Schwierz, F. Graphene Transistors: Status, Prospects, and Problems. *Proc. IEEE* **2013**, *101*, 1567–1584. [CrossRef]
3. Novoselov, K.S.; Geim, A.K.; Morozov, S.V.; Jiang, D.; Zhang, Y.; Dubonos, S.V.; Grigorieva, I.V.; Firsov, A.A. Electric field effect in atomically thin carbon films. *Science* **2004**, *306*, 666–669. [CrossRef] [PubMed]
4. Jiao, L.Y.; Zhang, L.; Wang, X.R.; Diankov, G.; Dai, H.J. Narrow graphene nanoribbons from carbon nanotubes. *Nature* **2009**, *458*, 877–880. [CrossRef] [PubMed]
5. Li, X.L.; Wang, X.R.; Zhang, L.; Lee, S.W.; Dai, H.J. Chemically derived, ultrasmooth graphene nanoribbon semiconductors. *Science* **2008**, *319*, 1229–1232. [CrossRef] [PubMed]
6. Schmidt, H.; Giustiniano, F.; Eda, G. Electronic transport properties of transition metal dichalcogenide field-effect devices: Surface and interface effects. *Chem. Soc. Rev.* **2015**, *44*, 7715–7736. [CrossRef] [PubMed]
7. Li, S.L.; Tsukagoshi, K.; Orgiu, E.; Samorì, P. Charge transport and mobility engineering in two-dimensional transition metal chalcogenide semiconductors. *Chem. Soc. Rev.* **2016**, *45*, 118–151. [CrossRef] [PubMed]
8. Hong, Y.K.; Liu, N.; Yin, D.; Hong, S.; Kim, D.H.; Kim, S.; Choi, W.; Yoon, Y. Recent progress in high-mobility thin-film transistors based on multilayer 2D materials. *J. Phys. D Appl. Phys.* **2017**, *50*, 164001. [CrossRef]
9. Kwon, J.; Hong, Y.K.; Han, G.; Omkaram, I.; Choi, W.; Kim, S.; Yoon, Y. Giant Photoamplification in Indirect-Bandgap Multilayer MoS_2 Phototransistors with Local Bottom-Gate Structures. *Adv. Mater.* **2015**, *27*, 2224–2230. [CrossRef] [PubMed]
10. Zhang, W.; Huang, J.K.; Chen, C.H.; Chang, Y.H.; Cheng, Y.J.; Li, L.J. High-gain phototransistors based on a CVD MoS_2 monolayer. *Adv. Mater.* **2013**, *25*, 3456–3461. [CrossRef] [PubMed]
11. Kwon, H.; Choi, W.; Lee, D.; Lee, Y.; Kwon, J.; Yoo, B.; Grigoropoulos, C.P.; Kim, S. Selective and localized laser annealing effect for high-performance flexible multilayer MoS_2 thin-film transistors. *Nano Res.* **2014**, *7*, 1137–1145. [CrossRef]
12. Kim, S.; Konar, A.; Hwang, W.S.; Lee, J.H.; Lee, J.; Yang, J.; Jung, C.; Kim, H.; Yoo, J.B.; Choi, J.Y.; et al. High-mobility and low-power thin-film transistors based on multilayer MoS_2 crystals. *Nat. Commun.* **2012**, *3*, 1011. [CrossRef] [PubMed]
13. Late, D.J.; Liu, B.; Matte, H.; Dravid, V.P.; Rao, C.N.R. Hysteresis in Single-Layer MoS_2 Field Effect Transistors. *ACS Nano* **2012**, *6*, 5635–5641. [CrossRef] [PubMed]
14. Guo, Y.; Wei, X.L.; Shu, J.P.; Liu, B.; Yin, J.B.; Guan, C.R.; Han, Y.X.; Gao, S.; Chen, Q. Charge trapping at the MoS_2-SiO_2 interface and its effects on the characteristics of MoS_2 metal-oxide-semiconductor field effect transistors. *Appl. Phys. Lett.* **2015**, *106*, 5. [CrossRef]
15. Qiu, H.; Pan, L.J.; Yao, Z.N.; Li, J.J.; Shi, Y.; Wang, X.R. Electrical characterization of back-gated bi-layer MoS_2 field-effect transistors and the effect of ambient on their performances. *Appl. Phys. Lett.* **2012**, *100*, 3. [CrossRef]
16. Radisavljevic, B.; Radenovic, A.; Brivio, J.; Giacometti, V.; Kis, A. Single-layer MoS_2 transistors. *Nat. Nanotech.* **2011**, *6*, 147–150. [CrossRef] [PubMed]
17. Liu, H.; Xu, K.; Zhang, X.; Ye, P.D. The integration of high-k dielectric on two-dimensional crystals by atomic layer deposition. *Appl. Phys. Lett.* **2012**, *100*, 152115. [CrossRef]
18. Yang, J.; Kim, S.; Choi, W.; Park, S.H.; Jung, Y.; Cho, M.H.; Kim, H. Improved growth behavior of atomic-layer-deposited high-k dielectrics on multilayer MoS_2 by oxygen plasma pretreatment. *ACS Appl. Mater. Interaces* **2013**, *5*, 4739–4744. [CrossRef] [PubMed]
19. McDonnell, S.; Brennan, B.; Azcatl, A.; Lu, N.; Dong, H.; Buie, C.; Kim, J.; Hinkle, C.L.; Kim, M.J.; Wallace, R.M. HfO_2 on MoS_2 by Atomic Layer Deposition: Adsorption Mechanisms and Thickness Scalability. *ACS Nano* **2013**, *7*, 10354–10361. [CrossRef] [PubMed]
20. Azcatl, A.; McDonnell, S.; Santosh, K.C.; Peng, X.; Dong, H.; Qin, X.; Addou, R.; Mordi, G.I.; Lu, N.; Kim, J.; et al. MoS_2 functionalization for ultra-thin atomic layer deposited dielectrics. *Appl. Phys. Lett.* **2014**, *104*, 111601. [CrossRef]
21. Yang, W.; Sun, Q.Q.; Geng, Y.; Chen, L.; Zhou, P.; Ding, S.J.; Zhang, D.W. The Integration of Sub-10 nm Gate Oxide on MoS_2 with Ultra Low Leakage and Enhanced Mobility. *Sci. Rep.* **2015**, *5*, 11921. [CrossRef] [PubMed]
22. Park, S.; Kim, S.Y.; Choi, Y.; Kim, M.; Shin, H.; Kim, J.; Choi, W. Interface Properties of Atomic-Layer-Deposited Al_2O_3 Thin Films on Ultraviolet/Ozone-Treated Multilayer MoS_2 Crystals. *ACS Appl. Mater. Interaces* **2016**, *8*, 11189–11193. [CrossRef] [PubMed]

23. Liu, N.; Baek, J.; Kim, S.M.; Hong, S.; Hong, Y.K.; Kim, Y.S.; Kim, H.S.; Kim, S.; Park, J. Improving the Stability of High-Performance Multilayer MoS_2 Field-Effect Transistors. *ACS Appl. Mater. Interaces* **2017**, *9*, 42943–42950. [CrossRef] [PubMed]
24. Das, S.; Chen, H.-Y.; Penumatcha, A.V.; Appenzeller, J. High performance multilayer MoS_2 transistors with scandium contacts. *Nano Lett.* **2012**, *13*, 100–105. [CrossRef] [PubMed]
25. Lee, Y.; Park, H.; Kwon, J.; Inturu, O.; Kim, S. High-temperature electrical behavior of a 2D multilayered MoS_2 transistor. *J. Korean Phys. Soc.* **2014**, *64*, 945–948. [CrossRef]
26. Yang, W.F.; Lee, S.J.; Liang, G.C.; Eswar, R.; Sun, Z.Q.; Kwong, D.L. Temperature Dependence of Carrier Transport of a Silicon Nanowire Schottky-Barrier Field-Effect Transistor. *IEEE Trans. Nanotechnol.* **2008**, *7*, 728–732. [CrossRef]
27. Kufer, D.; Konstantatos, G. Highly Sensitive, Encapsulated MoS_2 Photodetector with Gate Controllable Gain and Speed. *Nano Lett.* **2015**, *15*, 7307–7313. [CrossRef] [PubMed]
28. Na, J.; Joo, M.K.; Shin, M.; Huh, J.; Kim, J.S.; Piao, M.; Jin, J.E.; Jang, H.K.; Choi, H.J.; Shim, J.H.; et al. Low-frequency noise in multilayer MoS_2 field-effect transistors: The effect of high-k passivation. *Nanoscale* **2014**, *6*, 433–441. [CrossRef] [PubMed]
29. Neamen, D.A. *Semiconductor Physics and Devices*, 2nd ed.; McGraw-Hill: New York, NY, USA, 2003; ISBN 0-256-20869-7.
30. Choi, W.; Cho, M.Y.; Konar, A.; Lee, J.H.; Cha, G.B.; Hong, S.C.; Kim, S.; Kim, J.; Jena, D.; Joo, J. High-detectivity multilayer MoS_2 phototransistors with spectral response from ultraviolet to infrared. *Adv. Mater.* **2012**, *24*, 5832–5836. [CrossRef] [PubMed]
31. Davis, S.; Carver, J. Oxygen chemisorption at defect sites in MoS_2 and ReS_2 basal plane surfaces. *Appl. Surf. Sci.* **1984**, *20*, 193–198. [CrossRef]
32. Cho, K.; Park, W.; Park, J.; Jeong, H.; Jang, J.; Kim, T.Y.; Hong, W.K.; Hong, S.; Lee, T. Electric Stress-Induced Threshold Voltage Instability of Multilayer MoS_2 Field Effect Transistors. *ACS Nano* **2013**, *7*, 7751–7758. [CrossRef] [PubMed]
33. Liu, H.; Ye, P.D. MoS_2 Dual-Gate MOSFET With Atomic-Layer-Deposited Al_2O_3 as Top-Gate Dielectric. *IEEE Electron Device Lett.* **2012**, *33*, 546–548. [CrossRef]
34. Ghibaudo, G. New Method For the Extraction of Mosfet Parameters. *Electron. Lett.* **1988**, *24*, 543–545. [CrossRef]
35. Rhyee, J.-S.; Kwon, J.; Dak, P.; Kim, J.H.; Kim, S.M.; Park, J.; Hong, Y.K.; Song, W.G.; Omkaram, I.; Alam, M.A.; et al. High-Mobility Transistors Based on Large-Area and Highly Crystalline CVD-Grown $MoSe_2$ Films on Insulating Substrates. *Adv. Mater.* **2016**, *28*, 2316–2321. [CrossRef] [PubMed]
36. Chang, H.-Y.; Zhu, W.; Akinwande, D. On the mobility and contact resistance evaluation for transistors based on MoS_2 or two-dimensional semiconducting atomic crystals. *Appl. Phys. Lett.* **2014**, *104*, 113504. [CrossRef]
37. Xu, Y.; Minari, T.; Tsukagoshi, K.; Chroboczek, J.A.; Ghibaudo, G. Direct evaluation of low-field mobility and access resistance in pentacene field-effect transistors. *J. Appl. Phys.* **2010**, *107*, 114507. [CrossRef]
38. Kwon, H.-J.; Jang, J.; Kim, S.; Subramanian, V.; Grigoropoulos, C.P. Electrical characteristics of multilayer MoS_2 transistors at real operating temperatures with different ambient conditions. *Appl. Phys. Lett.* **2014**, *105*, 152105. [CrossRef]